

BLADE LOADING EFFECTS ON AXIAL TURBINE TIP LEAKAGE VORTEX DYNAMICS AND LOSS

Arthur C. Huang

Gas Turbine Laboratory
Massachusetts Institute of Technology
Cambridge, Massachusetts 02139
arthuang@mit.edu

Edward M. Greitzer

Gas Turbine Laboratory
Massachusetts Institute of Technology
Cambridge, Massachusetts 02139
greitzer@mit.edu

Choon S. Tan

Gas Turbine Laboratory
Massachusetts Institute of Technology
Cambridge, Massachusetts 02139
choon@mit.edu

Eugene F. Clemens

Turbine Aerodynamics
Rolls-Royce Corporation
Indianapolis, IN 46241
eugene.f.clemens@rolls-royce.com

Steven G. Gegg

Turbine Aerodynamics
Rolls-Royce Corporation
Indianapolis, IN 46241
steven.g.egg@rolls-royce.com

Edward R. Turner

Turbine Aerodynamics
Rolls-Royce Corporation
Indianapolis, IN 46241
edward.r.turner@rolls-royce.com

ABSTRACT

*Numerical simulations have been carried out to define the loss generation mechanisms associated with tip leakage in unshrouded axial turbines. Tip clearance vortex dynamics are a dominant feature of two mechanisms important in determining this loss: (i) decreased swirl velocity due to vortex line contraction in regions of decreasing axial velocity, i.e., adverse pressure gradient, and (ii) vortex breakdown and reverse flow in the vortex core. The mixing losses behave differently from the conventional view of flow exiting a turbine tip clearance. More specifically, it is shown, through control volume arguments and computations, that as a swirling leakage flow passes through a pressure rise, such as in the aft portion of the suction side of a turbine blade, the mixed-out loss can **either** decrease or increase. For turbines the latter typically occurs if the deceleration is large enough to initiate vortex breakdown, and it is demonstrated that this can occur case in modern turbines. The effect of blade pressure distribution on clearance losses is illustrated through computational examination of turbine blades with forward loading at the tip and with aft loading. A 15% difference in leakage loss is found between the two, due to lower clearance vortex deceleration (lower core static pressure rise) with forward loading and hence lower vortex breakdown loss. Additional computational experiments, carried out to define the effects of blade loading, incidence, and solidity, are found to be consistent with the proposed ideas linking blade pressure distribution, vortex breakdown and turbine tip leakage loss.*

NOMENCLATURE

AR Duct exit-to-inlet area ratio

C_p Pressure rise coefficient; $\Delta p / \frac{1}{2} \rho U^2$

H Duct height

S Swirl number; $u_{e,\theta} / u_s \approx \Gamma / 2\pi r_e u_s$

T Temperature

U_s, U_θ Velocity in freestream aligned with core axis, swirl direction

g Clearance height

\dot{m} Mass flow

p Pressure
 r_e Vortex core edge radius
 s Specific entropy
 t Time
 u_s, u_θ Velocity in vortex core aligned with core axis, swirl direction
 $u_{e,\theta}$ Swirl velocity at vortex core edge
 VR Vortex core velocity ratio; u_s/U_s
 W Duct width
 x/c Axial position / axial chord
 Δh_t Turbine stagnation enthalpy rise
 Γ Circulation
 Φ Dissipation function
 ρ Density
 σ Solidity; c/p , where c = blade chord, p = blade pitch
 τ Integration variable
 ξ Loss coefficient; $T\Delta s/\Delta h_t$ for turbines, $T\Delta s/V_{exit}^2$ for duct computations

INTRODUCTION

The leakage flow through the radial clearance between the tip of the rotating blades and the stationary casing is an important turbomachinery loss source. For an axial turbine, the decrease in efficiency from this loss is roughly proportional to clearance/span for a given design, [1], with proportionality levels between 1 to 3. Typical clearances for axial turbines lie in the range of 1-2% clearance/span [2] so the clearance loss for an unshrouded turbine is about one-third of the total loss [1, 3].

The characteristics of clearance flow over flat-tipped blades have been well-described [1, 4]. Flow enters on the pressure side. With a sharp corner a separation bubble forms on the tip at the pressure side corner. If the blade thickness to clearance ratio is greater than approximately 2, the flow will reattach [5] before exiting the clearance gap. At the gap exit the clearance flow and free stream velocities are not aligned and a shear layer (vortex sheet) exists between clearance and mainstream flows, which rolls up into a vortex.

A standard approach in describing the leakage flow is to divide the process into two fluid dynamic modules [6–8]. The first considers the flow passing through the gap. The second considers the interaction between the leakage flow and the mainstream.

For the first module the stagnation-to-static pressure ratio, including any losses, determines the state at the gap exit. In this connection, Heyes and Hodson, [7], building on the control volume model of Moore and Tilton, [2], developed a method to estimate the gap flow exit angle and velocity, given the static pressure at gap inlet and exit. Their analysis compared well with low speed turbine cascade data.

The second dynamic module, addressing what happens to the flow *once it exits the gap*, is the focus of this work. It has been found that the loss within the tip gap is only 10-15% of the total tip clearance loss, so that 85-90% of the clearance loss is tied to this second module [8]. Different approaches for describing the mixing process exist, from control volume [6] to three-dimensional calculation. The simplest clearance loss correlations assume the tip loss slope, i.e., the change in clearance loss for a given change in clearance, is independent of turbine design, but there are also correlations which link the clearance loss to the blade exit angle [9]. In the literature, however, there does not appear to be either broad assessment of the simpler models or more in-depth synthesis of the fluid dynamic processes using numerical simulation. In particular, a clear definition of loss sources and the physical mechanism by which they are related to blade design does not exist.

The contribution of this paper is to show the effect of blade loading on the tip clearance vortex, on its mixing with the mainstream flow, and on the generation of turbine tip clearance losses. There are both quantitative and qualitative aspects of the contribution. For the former, it is recognized that the specific results for mixing loss can depend on details of the turbine geometry as well as the computational procedures. For the latter, however, the concepts, the central physical processes, and the connection to blade design, appear broadly applicable. In our view it is this aspect that is the more important.

The scope of the paper is as follows: We first examine a subsonic high pressure turbine to illustrate general features (e.g., length scale, loss magnitude) of tip clearance vortex mixing. We then show, through analysis and computation, that for vortex mixing downstream of a pressure rise, such as can occur near the latter portion of the blade suction surface, the mixed out loss first decreases and then increases. The initial decrease is associated with the contraction (shortening) of vortex lines and the consequent decrease in swirl velocity. The increase is associated with vortex breakdown. We then describe the implementation of a hypothesis, based on these two mechanisms, that reducing the pressure rise experienced by the tip vortex would reduce the losses associated with vortex breakdown

and thus the overall clearance losses. Finally, several design change comparisons incorporating this idea are shown computationally to provide the desired decrease in tip clearance loss.

GENERAL FEATURES OF TURBINE TIP LEAKAGE VORTICES

To introduce the flow features to be explored, computations were carried out for a representative subsonic high pressure turbine blade at tip clearances from 0 to 2% of span. The calculations were done for a single rotating blade with a constant area duct upstream and downstream. The shroud was stationary. A hybrid mesh was used, with a structured mesh in the mainstream and an unstructured prism mesh at the center of the tip gap. Table 1 shows the parameters of the mesh. The inlet conditions were determined from a separate calculation including both stator and rotor and using a mixing plane interface. The exit static pressure was defined by holding hub exit static pressure constant as clearance was varied, with simple radial equilibrium used to provide the radial pressure distribution. Periodic boundary conditions linked the circumferential sides of the domain. No-slip, adiabatic wall boundary conditions were used for the solid surfaces. The Reynolds-Averaged Navier Stokes (RANS) equations were solved using ANSYS FLUENT, a commercial finite volume code. Turbulence was modeled using the Spalart-Allmaras turbulence model [10] and the inlet turbulence level was set to 10%. The mesh had an average y^+ equal to 1 in the first cell from the surface, and a separate calculation using twice the number of cells showed that the solution was insensitive to the grid. The appendix gives additional information related to grid convergence and the choice of turbulence model.

Figure 1a shows the suction surface isentropic Mach number at 80% span as a function of axial position, x/c , and Figure 1b shows the vortex swirl number and the vortex centerline velocity, denoted here as the "core axis velocity"¹, nondimensionalized by the average exit velocity, also as a function of x/c . At 75% axial chord, the mainstream velocity decreases (Figure 1a), but the core axis vortex velocity decreases more rapidly, becoming negative downstream of the trailing edge (Figure 1b). The locations of negative flow and of peak vortex core swirl number are also close together.

The flow field associated with the clearance vortex is portrayed in Figure 2, which gives contours of the velocity normal to several planes perpendicular to the blade suction surface. The velocity normal to the planes is a good approximation to the core axis velocity, since the planes are nearly normal to the vortex core. The white regions in the fourth and fifth planes indicate regions of reversed flow; the level of the negative velocity can be seen in figure 1b². Figures 1 and 2 show the quantitative connection between deceleration on the suction surface, or equivalently, rise in static pressure, and the behavior of the leakage flow vortex. We will define this connection in more depth below, including the link between vortex dynamics and mixing loss.

ASSESSMENT OF CONTROL VOLUME DESCRIPTION OF TIP CLEARANCE LOSSES

In assessing the effect of pressure gradient³ on vortex dynamics and mixing losses it is useful to begin with constant area mixing as a baseline. This provides a framework for discussion of mixing losses and a touchstone in comparing more complex situations where there are different pressure levels during the mixing process.

An approximate formulation of tip leakage as a mixing channel flow, with two streams of different properties, and one mass flow much larger than the other has been given by Denton [6] and others [12, 13]. The two streams enter the constant area control volume, mix, and exit at a uniform state. The entropy generated within the control volume due to irreversible processes is stated in Equation 1 [14].

$$T\Delta s_{gen} = \frac{\dot{m}_2}{\dot{m}_1} \left(\frac{1}{2} [U_{2,y}^2 + (U_1 - U_{2,x})^2] + c_p T \int_T^{T_2} \left(\frac{1}{T} - \frac{1}{\tau} \right) d\tau \right) \quad (1)$$

¹The core axis velocity, denoted by the subscript s , is the velocity on the vortex centerline. The tip vortex core axis is not aligned with the axis of the turbomachine, and "core axis velocity" is used here to distinguish the velocity in the direction of the vortex core axis from the "axial velocity", or velocity along the turbomachine axis of rotation.

²The region of reversed flow occurs behind the trailing edge, in x/c coordinates, in Figures 1b and 2. In Figure 2 even though the *intersections* of the last two planes with the blade are at values of $x/c \leq 1$, the vortex center on these planes is actually at a value of x/c larger than unity.

³The equations that describe changes in vorticity do not have a term involving pressure, and it is not consistent to use features of the pressure field in motivating the vorticity behavior [11]. In a turbomachinery design context, however, much of the thinking about blade performance is in terms of static pressure. It thus seems simpler to use the implied connection (through Bernoulli) of pressure and velocity and refer to changes in pressure, rather than to keep having to put the point in terms of velocity variations and then make the connection to the pressure distribution.

The terms in the square brackets represent dissipation of kinetic energy. The first term corresponds to loss of kinetic energy associated with the cross flow velocity. The second corresponds to the loss in kinetic energy from equilibrating leakage and mainstream flow speeds in the main flow direction. The integral represents irreversibility resulting from the static temperature difference between the two streams. This term is small in the present situation (less than 5% of the total loss) because the leakage and the main stream flows start at the same stagnation temperature.

The interest here is in the effect of pressure level on tip leakage mixing loss. As an initial step we compare the control volume description with numerical simulations of flow injection into rectangular nozzles and diffusers with area ratios (from inlet of the nozzle or diffuser to outlet) ranging from 0.5 to 1.7. Slip wall boundary conditions are used so there are no viscous stresses at the walls. The comparison made is between a control volume estimation of mixing loss and the difference between the inlet entropy flux and the mixed out entropy flux at the conditions at the domain outlet. This mixed out state is determined via constant area control volume analysis applied at the domain outlet.

The control volume estimate for losses was obtained applying Equation 1 over the injection slot exit and mixing the leakage flow from an elementary area at a given axial location to the midspan velocity at that axial location.

Figure 3 shows the computational domain for a nozzle with exit-to-inlet area ratio (AR) 0.8 and constant duct height H . The duct width, W , is equal to the height at the inlet ($x/H = 0$) and decreases (or increases) to the outlet width between $x/H = 1$ and 2. Flow is injected from the indicated thin rectangular slot, where the dimensions are $0.02H$ by H , to approximate a tip leakage flow.

Figure 4a shows the mixed out loss as a function of AR for a basically incompressible flow (inlet-stagnation-pressure-to-outlet-static-pressure ratio of 1.05). The injection is normal to the free stream. The loss is non-dimensionalized by product of the injected mass flow and the square of the duct exit velocity, to give a metric for the loss per unit injected flow.

For a constant area duct ($AR=1$), the control volume and the numerical simulation agree (as would be expected) to within 2%; this is basically a check on the accuracy of the simulation. For $AR < 1$, the mixing losses are underestimated by the control volume analysis compared to the numerical simulation, whereas for $1 < AR < 1.5$, the mixing losses are overestimated by the control volume analysis. Figure 4a shows that at $AR = 1.3$, however, the computed rate of change of loss for the simulation becomes larger than for the control volume and for $AR > 1.5$ the control volume analysis again underestimates the loss.

The reason for the difference in calculated loss is that the control volume approach does not appropriately account for the change in pressure experienced by the injected flow prior to complete mixing. The control volume assumption is that the injected flow mixes out after entering the mainstream in what is, because of the large ratio of mainstream to leakage flow, essentially a constant pressure process. In reality the injected flow passes through a pressure change during mixing with the mainstream so that a portion of the mixing occurs at a pressure different from the clearance exit pressure. This is a situation often found in turbomachinery, and the effect of pressure level on wake mixing is well known, e.g. [6, 14]. What is different in the present situation is that, over the area ratios from less than one to 1.5 or so, the trend in mixing loss with area ratio is opposite to that for a wake in a pressure gradient. Specifically, *the mixed out loss of a vortex can decrease as the vortex passes through a pressure rise and can increase as the vortex passes through a drop in pressure*, in contrast to the behavior of a wake. We describe the physical mechanism for this in the next section.

Coming back to Figure 4a, what will also be shown subsequently is that the loss behavior for $AR > 1.4$, roughly, is dominated by vortex breakdown, defined here as a situation in which the flow in the vortex core reverses and the core exhibits a substantial change in size. As described in the literature, a vortex core swirl number near 1.4 (the exact value depends on velocity profile and geometry) marks the occurrence of this breakdown [14, 15]. This is seen in Figure 4b in which the vortex core swirl number is plotted as a function of duct area ratio. Figures 4a and 4b show that as the vortex is exposed to larger pressure rises the swirl number and the losses show a rapid increase.

COMPARISON OF THE EFFECT OF PRESSURE LEVEL ON WAKE AND VORTEX MIXING LOSSES

We can demonstrate the effect of pressure level on mixed out loss for a general flow non-uniformity in a wake and in a vortex. For the former a pressure rise increases the wake velocity defect as seen in Equation 2, the differential form of the one-dimensional momentum equation.

$$\frac{du}{u} = -\frac{dp}{\rho u^2} \quad (2)$$

The fractional decrease in velocity due to the pressure rise is inversely proportional to the dynamic pressure, so the change in wake

velocity for a given incremental pressure rise is greater than the free stream velocity, and the wake decelerates more than the freestream. The mixed-out loss scales as the velocity defect squared, as in Equation 1.

A vortex in an axial pressure gradient behaves differently from a wake, because of the radial pressure gradient that exists in a swirling flow. Equation 3 describes the difference between far field pressure, p_∞ , and core centerline pressure, $p(x,0)$, of a Rankine vortex⁴ as a function of the non-dimensional circulation, $\Gamma/4\pi^2 r_e^2$. For a given increase in freestream pressure, i.e., given deceleration of the free stream, there is a larger increase in core centerline pressure than with no swirl because the core is slowed down and the core radius increases, as in Equation 4. The vortex core thus sees a larger pressure change, and the core axial velocity thus decreases more, than the axial velocity of a wake at the same initial velocity and imposed far field pressure rise. This effect tends to increase the axial velocity defect, and thus the mixed out loss, compared to a wake.

$$p(x,0) = p_\infty - \rho \left(\frac{\Gamma^2}{4\pi^2 r_e^2} \right) \quad (3)$$

$$\frac{d[p_\infty - p(x,0)]}{2\pi^2(\Gamma r_e)^2} = \frac{dr_e}{r_e} \quad (4)$$

There is, however, another effect of a pressure rise associated with the swirl velocity. Deceleration of the core means the axial vortex lines shrink in length, or, equivalently that there is an increase in core radius. Neglecting, for the moment, viscous effects, Kelvin's Theorem states that a ring of fluid particles around the vortex keeps its circulation but, because of the increase in radius, suffers a decrease in swirl velocity. Because there is a large region of flow with swirl, *the mixed-out loss* (defined as the loss in constant area mixing to a state of uniform axial flow) *can depend more strongly on the dissipation of swirl kinetic energy than on the dissipation of kinetic energy associated with the velocity along the core axis*. If so the mixed-out loss decreases as the pressure rises.

Figure 5 shows the effect of a far field pressure rise on the core axis velocity defect $(U_s - u_s)/(U_s - u_s)_{inlet}$, swirl velocity $u_{\theta,e}/U_{s,inlet}$, and mixed-out loss $\Delta s_{exit\ mixed-out}/\Delta s_{inlet\ mixed-out}$ for a wake and a vortex. The wake and the vortex have the same initial value of core axis velocity ratio between core and free stream, $VR = u_s/U_s = 0.6$. The vortex has an initial core swirl number, $S = \Gamma/2\pi r_e u_s$, of 0.83, conditions representative of a turbine tip vortex. The vortex calculations are based on a one-dimensional model for vortex core flows [14, 15], which has been shown to capture the features of interest here.

The wake velocity defect and the wake mixed-out loss both increase with pressure rise. For the vortex, as the pressure rises, the core velocity defect increases more sharply than for the wake, but the swirl velocity decreases. The dominant contribution to the change in mixed-out loss comes from the change in swirl velocity in the freestream, since the vortex core mass flow is much smaller than the free stream mass flow, and thus the mixed-out loss decreases. The curves corresponding to the vortex can only be continued until the value of C_p corresponding to stagnation of the core flow, beyond which the control volume is inapplicable [15].

To assess vortex core and mixed-out loss behavior for larger nondimensional pressure rises at which reversed flow can be found, computations of vortices in axisymmetric expansions have been performed using FLUENT. The inlet velocity is specified to be that of a Burger's vortex, which has similar qualitative features to the Rankine vortex but is defined by a smoothly varying velocity distribution⁵ [15]. The initial core radius r_e is 0.1 of the duct radius, so the initial ratio of vortex core area to free stream area is 1%. An outflow boundary condition is used at the duct exit. The outer boundary is a slipwall to minimize losses unrelated to vortex behavior. Turbulence is modeled using the RNG k- ϵ model [16], and the vortex core Reynolds number, based on core radius and freestream velocity, is 8×10^4 , approximately the Reynolds number of the clearance vortex in the subsonic high pressure turbine described above. The choice of turbulence model is discussed in the appendix.

Figure 6 shows the change in mixed-out loss between the duct inlet and exit plane. The results are normalized by the inlet mixed-out loss, as a function of the static pressure rise coefficient along the duct outer radius. Results are presented for vortices with initial velocity ratio 0.6 and swirl numbers 0.0 (a wake), 0.42, and 0.83. The wake mixed-out loss increases monotonically with pressure rise. The vortex mixed-out loss vortices decreases for $0 < C_p = \Delta p(r = R_{wall})/\frac{1}{2}\rho U_s^2 < 0.3$, because of vortex line contraction and decreased swirl velocity.

⁴A Rankine vortex has a core of uniform vorticity ($u_\theta = \Omega r$ where Ω is independent of radius) surrounded by irrotational flow. The velocity in the core aligned with the core axis direction u_s is uniform but may be different from the velocity along this direction in the surrounding irrotational flow, U_s .

⁵A Burger vortex has swirl velocity $u_\theta = \frac{\Gamma}{2\pi r_e} \left\{ 1 - \exp \left[1.26 \left(\frac{r}{r_e} \right)^2 \right] \right\}$. The velocity in the core axis direction is u_s for $r < r_e$ and U_s for $r > r_e$.

Figure 7a shows contours of swirl velocity (normalized by freestream inlet velocity) for $C_p = 0.05, 0.19,$ and 0.31 (conditions A, B, and C in figure 6). As the pressure rise increases, the swirl velocity ratio decreases from 0.32 to 0.27 , with a consequent drop in mixed-out loss. From Figure 6, however, the loss for the $S = 0.83$ vortex begins to increase at $C_p = 0.3$ and at $C_p = 0.38$, the exit mixed-out loss becomes larger than the inlet mixed-out loss.

The steep loss increase in Figure 6 is due to vortex breakdown and flow reversal. Figure 7b shows contours of core axis velocity ratio for $S = 0.83$ and outer wall pressure rises $C_p = 0.31, 0.37,$ and 0.42 (conditions C, D, and E in figure 6). For $C_p = 0.31$, the reversed flow region occupies 0.07% of the duct area, but for $C_p = 0.42$ the region of reversed flow has grown by an order of magnitude to occupy 0.8% of the duct area.

The calculations show smaller loss changes than given by the control volume analysis in Figure 5 because viscous effects mix the flow before and during the area expansion. The qualitative behaviors for the two descriptions, however, are in accord. Both show that a vortex which passes through a pressure rise less than that which causes vortex core stagnation experiences a decrease in mixed-out loss. As the pressure rise increases past a critical value, the vortex breaks down and the mixed-out loss increases because of increased flow reversal. This behavior is consistent with the changes in loss observed in the rectangular duct computations (Figures 4a and 4b) for $AR > 1.5$, which have swirl number above 1.4 , the value indicative of vortex breakdown.

IMPLICATIONS FOR, AND COMPARISONS OF, MIXING LOSSES IN TURBINE AND COMPRESSOR TIP CLEARANCE FLOWS

Compressor tip clearance flows have initial swirl numbers less than 0.5 and the dynamical effects of swirl can thus often be neglected with the leakage flow approximated (with some success) as a wake in a pressure gradient [17]. We have shown above, however, that this approximation is not appropriate for turbine tip flows and that the swirl dynamics need to be accounted for. In this context, Figure 8 shows the behavior of the mixing loss for vortices of different swirl numbers and core velocity ratios. The figure gives contours of the ratio of incremental increase in normalized mixing loss (defined as mixed-out loss divided by inlet mixed-out loss) to incremental pressure rise⁶. The mass flow ratio, vortex core to free stream, is 1% , representative of tip leakage vortices. The vertical axis is the locus of wake initial states (swirl number equal to zero).

Figure 8 shows the regions of the swirl number-velocity ratio plane in which, in accord with the examples in Figures 4, 5, and 6, the change in mixed-out loss with pressure rise can be greater or less than zero. The division between the two is given by the heavy line that starts at the upper left hand corner of the plot. The two competing effects implied by the figure can be referred to as wake-like and vortex-like behaviors. Below the heavy line, for a given swirl number, the loss derivative increases as the velocity ratio decreases and the flow becomes more "wake-like". This is the familiar behavior for a wake in a pressure gradient, with increased mixed-out loss if the pressure rises. For a given initial velocity ratio, however, the loss derivative decreases as the swirl number increases, and the flow becomes more vortex-like, with the mixed-out loss decreasing as the pressure rises.

EFFECT OF BLADE PRESSURE DISTRIBUTION ON LEAKAGE LOSS

The above ideas about mixing losses in vortex core flows provide a framework to describe the effects of blade pressure distribution on tip clearance losses. For the subsonic HP turbine flowfield portrayed in Figure 2, the vortex undergoes a pressure rise large enough to cause vortex breakdown and flow reversal in the core. Further, the axisymmetric vortex calculations indicate that in the vortex breakdown regime, losses rise rapidly with pressure level. If so, there is a possibility for decreasing tip clearance loss by decreasing the pressure rise near the trailing edge, so the vortex is subjected to less deceleration. Implementing designs and diagnostic experiments that allow us to evaluate this hypothesis is the topic of the rest of the paper.

As an initial step in the assessment two blades were designed as modifications to the baseline blade. One incorporated a forward loaded tip section and the other an aft loaded tip section. Both blades performed the same overall work as the baseline to within 0.25% . With the forward loaded design the vortex had less deceleration and, with the aft loaded, more deceleration, compared to the baseline case of Figure 1. In the remainder of this section, the forward loaded, and aft loaded designs will be referred to as the F and A blades, respectively.

Figure 9a illustrates the A, B (baseline), and F tip section geometries. In shifting the loading from aft to forward, the blade camber was decreased and the suction surface flattened. The blade was re-stacked to include the new tip design, with the tip blended linearly into the 50% span airfoil shape. Meshes were generated with the same near-wall node spacing as the baseline, and simulations were carried out for clearances from $0-2\%$ under the same conditions as the baseline mid-loaded tip (see table 1).

⁶This can be regarded as a "loss derivative", $\Delta(\text{Normalized mixed-out loss})/\Delta C_p$, as the small change in normalized pressure, ΔC_p , approaches zero

Figure 9b gives the computed isentropic suction surface Mach number at 80% span, as a function of axial position for 0.5% clearance. This clearance was chosen the tip clearance vortex would have negligible impact on the loading at this spanwise location. The desired effect has been achieved in that between x/c of 0.75 and 1, the circled region in the figure, the negative slope of the suction surface isentropic Mach number is steeper for the A blade than for the F blade.

Figure 10a shows the clearance loss versus nondimensional tip clearance for the three blades. The F blade was found to have 9% less clearance loss than the baseline design and 15% less loss than the A blade. Stated differently, as the loading goes from forward to aft, the tip clearance loss slope, i.e., the percent change in loss for a 1% change in tip clearance, increases by 15%. This occurs despite a decrease in leakage mass flow, as indicated in Figure 10b which gives the clearance mass flow ratio (clearance flow divided by passage flow) for A, B, and F blades as a function of clearance. The F blade has 14% larger clearance mass flow than the A blade, so there is a 30% difference in mixing loss per unit leakage flow between F and A blades.

The bar chart in Figure 11 summarizes the trends for the three blades. The figure presents the loss per unit of leakage massflow, normalized by the computed value for the baseline blade, at 2% clearance, as well as results from the control volume loss analysis (tip leakage flow mixed-out at local suction surface velocity as in Equation 1). The loss within the gap, per unit leakage mass flow, decreases as the loading goes from aft to forward, but it is a small part of the overall loss and does not account for the change in loss. The control volume approach captures the qualitative effect of pressure distribution, namely that forward loading decreases the clearance loss, however, it underpredicts the change by a factor of nearly four, implying that additional effects need to be included.

Figure 12 shows features of the clearance vortex core evolution in more detail. Figure 12a gives the distribution of core centerline velocity, normalized by the average exit velocity as a function of axial position for the three blades. The aft loaded blade and the baseline both have negative velocities, whereas the forward loaded blade does not. The consequence of the different core deceleration is illustrated in Figure 12b, which gives the mixing loss (viscous dissipation outside of the boundary layers) per unit axial distance as a function of axial location for the A, B, and F blades. The A blade has 35% higher mixing loss per unit distance in the region $x/c = 1$ to 1.4, where there is breakdown of the tip clearance vortex and mixing out. Our inference from these results is that vortex breakdown is the major loss mechanism contributing to the difference in loss per unit leakage between the A and F blades.

Changes in the clearance vortex flow field between the differently loaded blades are portrayed in Figure 13, which shows the ratio of core axis velocity to exit velocity for the A and F blades as the color contours. For the A blade, the core centerline velocity is negative, dropping to -0.13 (Figure 12a), indicating reversed flow. For the F blade there is no flow reversal because the reduced pressure rise (Figure 9b) produces less deceleration of the vortex core.

Figure ?? compares contours of volumetric entropy generation rate⁷ in the F and A blade at the location of maximum entropy generation per unit axial distance, $x/c = 1.15$. The maximum local dissipation at this plane is a factor of two larger for the A blade than for the F blade, confirming that the increase in viscous dissipation between A and F blades occurs in the vortex breakdown region.

ADDITIONAL NUMERICAL EXPERIMENTS WITH DIFFERENT BLADE DESIGNS

The previous section contains the crux of the arguments that link the blade pressure distributions to the magnitudes of the tip clearance losses. To assess the ideas further, however, we have performed additional diagnostic design experiments. First, to achieve a larger change in loading distribution the three different tips were extruded into 2D blades for a rectilinear cascade. These are denoted by A2, B2, and F2 in Figure 15. Figure 15a shows the isentropic suction surface Mach number distributions with larger differences than in Figure 9.

Results of this set of numerical experiments are given in terms of mixing loss per unit of leakage flow in Figure 15b. The losses are normalized with reference to the computed losses for the baseline two-dimensional blade, B2. The forward loaded cascade blade, F2, has only 50% of the mixing loss per unit leakage flow of the aft loaded blade, A2. The change in loss is associated with a larger difference in vortex behavior than in the previous section; the difference in minimum core velocity ratio between forward and aft loaded blades increases from 0.15 for the A and F blades (Figure 12a) to 0.25 for the A2 and F2 blades. Finally, the estimated mixing loss given by the control volume analysis agrees qualitatively with the trends but is a factor of two low in terms of capturing the quantitative changes.

Second, changes in incidence angle were used to assess the effects of pressure distribution on vortex dynamics and clearance loss. The baseline cascade was examined at inlet angles of nominal and plus and minus 10 degrees. The positive incidence angles front load the blades. Figure 16a shows isentropic suction surface Mach number. The difference in pressure distribution is marked in the front third of the blade. The difference in pressure distribution near the rear of the blade is much less pronounced, but the pressure

⁷The volumetric viscous entropy generation is given by $\rho \frac{ds}{dt} = \frac{\Phi}{T}$, where Φ is the dissipation function [18], and is non-dimensionalized as $\frac{T_{exit} \rho V \frac{ds}{dt}}{\dot{m}_{main} \Delta h_t}$, where V is the domain volume.

rise in the aft portion of the blade does decrease as the incidence increases. Figure 16b, which again shows computations and control volume analysis, gives the mixing loss per unit of mass flow, showing a 17% decrease between the low incidence (aft-loaded) and high incidence (forward-loaded) cases.

The third study, using solidity as a diagnostic, was carried out with the original three-dimensional baseline (B) blade. This was examined at solidities from 0.88 to 1.07, implemented by increasing the number of blades in the annulus. For given turbine work per unit mass flow, increasing the solidity decreases the blade loading. The tip clearance loss decreased by 15% over the range and the loss per unit leakage flow decreased by approximately 50%.

Figure 17a connects the change in loss per unit leakage flow to tip vortex breakdown. The figure shows the isentropic suction side Mach number. The lower solidity produces a larger decrease in Mach number, in other words larger pressure rise, at the rear of the suction surface. The change in mixed-out loss is shown in Figure 17b; the control volume analysis again is seen to underpredict the actual changes in loss.

The changes in vortex core behavior at the different solidities are given in Figures 18a and 18b. The former shows the ratio of vortex core centerline velocity to exit velocity. For lower solidity the core decelerates more, with reverse flow occurring in the low solidity (0.88) and baseline solidity (0.97), and no reverse flow in the highest solidity examined (1.07). Figure 18b shows the tip clearance mixing loss per unit axial distance, with the highest value for the low solidity turbine.

CONCLUSIONS

In this paper, we propose a physical mechanism that links the suction surface pressure distribution and the tip clearance loss of an unshrouded axial turbine blade. From numerical simulations, the dynamics of the tip clearance vortex has been found to play an important role in determining tip clearance loss. A new result is that for incremental pressure rises along the direction of the vortex axis, deceleration of the vortex core can *increase or decrease* the mixed-out loss of a vortex depending on the swirl number ($u_s/u_{e,\theta}$) and the core velocity ratio (u_s/U_s). Leakage flow vortices with low values of both of these (roughly below 0.5 for both, denoting weak swirl and a substantial velocity defect compared to the free stream) will exhibit the familiar behavior of a wake in a pressure gradient, with increased mixing losses for an incremental pressure rise. Leakage flow vortices with high values of both of these (roughly above 0.5 for both, denoting strong swirl and a small velocity defect compared to the free stream) will exhibit the converse, vortex-like, behavior, with decreased mixing losses for an incremental pressure rise. In general, compressor tip flows tend to be the former type and turbine tip flows the latter.

For *pressure rises large enough to stagnate the vortex core flow*, mixed-out loss increases rapidly with pressure level. The calculations reported here demonstrate that the pressure rises at the rear section of subsonic high pressure turbines are sufficient to cause such stagnation (vortex breakdown). These results implied that changes in the suction surface pressure distribution, specifically a reduction in the adverse pressure gradient at the rear of the blade, could reduce, or eliminate, the vortex breakdown and thus reduce the tip clearance losses.

To assess this hypothesis, designs were (numerically) carried out in which a baseline blade tip section was changed to load the front of the blade and then to load the rear. The former reduced the clearance loss by 15% compared to the latter. Further diagnostic computations, which made use of the effects of (one by one) blade loading distribution, incidence, and solidity as instruments to change the level of pressure rise experienced by the clearance vortex are also shown to corroborate the basic idea expressed in the previous paragraph.

ACKNOWLEDGMENT

The support of the Rolls-Royce Whittle Fellowship is gratefully acknowledged. The authors also wish to thank N. Cumpsty and S. Gallimore for helpful comments, and K. Weber and M. Creason for their help with the computations, S. Mazur for sharing his computational results, and the reviewers for the time and thought put into the review comments.

APPENDIX - GRID CONVERGENCE AND CHOICE OF TURBULENCE MODEL

In this Appendix we address questions of possible effects of grid convergence, turbulence model, and inlet turbulence level on the computational results and thus on the conclusions. We show, from the results of additional simulations, that the central fluid dynamic and thermodynamic behavior developed in the paper are not sensitive to the grid or the turbulence model that was used. More precisely, although there are *quantitative* differences, these are small (approximately 10% for the detailed metrics and several percent for the overall features) and the *qualitative differences with conventional wake behavior are unchanged*.

The first question is the sensitivity of solution features to the grid. To assess this, computations were run for the baseline (B) blade using a grid with twice as many cells as the computations reported in the main part of the paper (6 million for the fine grid versus 2.8 million for the original grid). This was done for both the zero clearance and the 2% clearance, the primary tip gap described in the computations. In comparing the results, we choose as metrics quantities important to the concepts addressed in the paper. Three overall metrics are tip leakage, leakage loss, and adiabatic efficiency. The first of these, the leakage, changed by only 3% between the original grid and fine grid. The leakage loss, i.e., the *difference* in entropy generation between zero clearance and 2% clearance) also changed by 3%. This was in fact the largest difference in the entropy generation distribution with x/c , for which the original and fine grid results tracked within this value until the exit of the domain. The adiabatic efficiency changed by approximately 0.25%.

Metrics that assess local fluid dynamic quantities are a more severe test of the extent to which grid convergence has been achieved. Two such quantities are the difference between the maximum and minimum value of the nondimensional vortex core axis velocity, and the vortex swirl number at the onset of flow diffusion, $u_{e,\theta}/u_x$, as indicated for example, in Figure 1 of the paper.

Vortex core axis velocity is critical in determining the mixing loss. The differences between the values of maximum and minimum vortex core axis velocity, with the original grid and with the fine grid, is 7%. The extent of the region of negative core axis velocity, which shows the capturing of reversed flow by the computations, was altered from 18% to 20% (in units of x/c), with the larger value corresponding to the fine grid, an 11% change. The vortex swirl number at the onset of diffusion was 1.16 with the original grid and 1.18 with the fine grid.

The changes in these various metrics are not large in a quantitative sense. Further, and more importantly for the findings and conclusions of the paper, there are no changes in the qualitative behavior of even the most sensitive of the metrics. These observations argue strongly that the grid used in the paper captures the quantities of interest in a representative and appropriate manner.

The second issue is turbulence modeling for vortex flows. As described in the literature (for example, [19], [20], [21], [22]) RANS calculations have been found to give useful representations of vortex flows, although they generally produce excessive diffusion of the vortex core. It is reported that Reynolds Stress Models (RSM) are the most accurate, followed by two equation methods (for example the RNG $k-\epsilon$ model and SST $k-\omega$ models), while the Spalart-Allmaras (S-A) model produces excess diffusion compared to the above [20]. For this reason, the RNG $k-\epsilon$ model was used for the calculation of vortices in axisymmetric ducts (Figure 6). The S-A model was chosen for the turbine computations because of its robustness. To assess the effect of turbulence model, computations were carried out on the A and F blades using the SST $k-\omega$ model [23]. The calculations with the S-A model gave estimates of a 16% difference in leakage loss between A and F blades, those with the SST $k-\omega$ model predicted a 20% difference. Because the S-A model provides the larger diffusion, it can be taken as a bounding case; diffusion and mixing work to weaken the vortex, making it less susceptible to flow reversal upon encountering a pressure rise. One might thus expect that vortices predicted by more accurate turbulence models may behave in a more inviscid manner and react more strongly to the pressure changes. In sum, inaccuracies due to turbulence model are small and are likely to lead to slight underestimates of the importance of the phenomena described in the paper; the S-A model can thus be regarded as conservative in this respect.

A possible third issue is inlet turbulence level. Computations were run for the B blade with inlet turbulence levels 1% and 10%, with the result being only a 1.2% change in leakage loss.

REFERENCES

- [1] Booth, T. C., 1985. "Importance of tip clearance flows in turbine design". In *Tip Clearance Effects in Axial Turbomachines*, VKI Lecture Series 1985-05. VKI.
- [2] Moore, J., and Tilton, J. S., 1988. "Tip leakage flow in a linear turbine cascade". *J. Turbomach.*, **110**(1), pp. 18–26.
- [3] Harvey, N. W., 2004. "Aerothermal implications of shroudless and shrouded blades". In *Turbine Blade Tip Design and Tip Clearance Treatment*, VKI Lecture Series 2004-02. VKI.
- [4] Bindon, J. P., 1989. "The measurement and formation of tip clearance loss". *J. Turbomach.*, **111**(3), pp. 257–263.
- [5] Krishnababu, S. K., Hodson, H. P., Dawes, W. N., Newton, P. J., and Lock, G. D., 2009. "Numerical and experimental investigation of tip leakage flow and heat transfer using idealised rotor-tip models at transonic conditions". *The Aeronautical Journal*, **111**(1141), pp. 165–186.
- [6] Denton, J. D., 1993. "Loss mechanisms in turbomachines". *J. Turbomach.*, **115**(4), pp. 621–656.
- [7] Heyes, F. J. G., and Hodson, H. P., 1993. "Measurement and prediction of tip clearance flow in linear turbine cascades". *J. Turbomach.*, **115**(3), pp. 376–382.
- [8] Yaras, M. I., and Sjolander, S. A., 1992. "Prediction of tip-leakage losses in axial turbines". *J. Turbomach.*, **114**(1), pp. 204–210.
- [9] Kacker, S. C., and Okapuu, U., 1982. "A mean line prediction method for axial flow turbine efficiency". *J. Eng. Power*, **104**(1), pp. 111–119.

- [10] Spalart, P. R., and Allmaras, S. R., 1994. “A one-equation turbulence model for aerodynamic flows”. *La Recherche Aerospatiale*, *I*(1), pp. 5–21.
- [11] Lighthill, M. J., 1963. “Introduction: Boundary-Layer Theory”. In *Laminar Boundary Layers*, L. Rosenhead, ed., Fluid Motion Memoirs. Oxford University Press.
- [12] Young, J. B., and Wilcock, R. C., 2002. “Modeling the air-cooled gas turbine: Part 2—coolant flows and losses”. *J. Turbomach.*, *124*(2), pp. 214–221.
- [13] Shapiro, A. H., 1953. *The Dynamics and Thermodynamics of Compressible Flow, I*. The Ronald Press Company.
- [14] Greitzer, E. M., Tan, C. S., and Graf, M. B., 2004. *Internal Flow*. Cambridge University Press.
- [15] Darmofal, D. L., Khan, R., Greitzer, E. M., and Tan, C. S., 2001. “Vortex core behaviour in confined and unconfined geometries: a quasi-one-dimensional model”. *J. Fluid Mech.*, *449*, pp. 61–84.
- [16] Yakhot, V., Orszag, S. A., Thangam, S., Gatski, T. B., and Speziale, C. G., 1992. “Development of turbulence models for shear flows by a double expansion technique”. *Physics of Fluids A: Fluid Dynamics*, *4*(7), pp. 1510–1520.
- [17] Khalid, S. A., Khalsa, A. S., Waitz, I. A., Tan, C. S., Greitzer, E. M., Cumpsty, N. A., Adamczyk, J. J., and Marble, F. E., 1999. “Endwall blockage in axial compressors”. *J. Turbomach.*, *121*(3), pp. 499–509.
- [18] Kundu, P. K., and Cohen, I. M., 2008. *Fluid Mechanics*. Elsevier Academic Press.
- [19] Krishnababu, S. K., Newton, P. J., Dawes, W. N., Lock, G. D., Hodson, H. P., Hannis, J., and Whitney, C., 2009. “Lessons learned from the numerical investigations on the vfe-2 configuration”. *Report: Understanding and Modeling Vortical Flows to Improve the Technology Readiness Level for Military Aircraft*.
- [20] Wells, J., 2009. “Effects of turbulence modeling on RANS simulations of tip vortices”. Master’s thesis, Virginia Polytechnic and State University, Blacksburg, VA, USA, August.
- [21] Escue, A., and Cui, J., 2010. “Comparison of turbulence models in simulating swirling pipe flows”. *Applied Mathematical Modelling*, *34*(10), pp. 2840–2849.
- [22] Revell, A., Iaccarino, G., and Wu, X., 2006. “Advanced rans modeling of wingtip vortex flows”. *Proceedings of the 2006 Summer Program, CTR*, pp. 73 – 86.
- [23] Menter, F. R., 1994. “Two-equation eddy-viscosity turbulence models for engineering applications”. *AIAA Journal*, *32*(8), pp. 1598–1605.
- [24] Khalid, S. A., 1995. “The effects of tip clearance on axial compressor pressure rise”. PhD thesis, Massachusetts Institute of Technology, Cambridge, MA, USA, May.

1 Tables

TABLE 1. Mesh parameters

Cell count (2% clr)	2.8×10^6
Avg blade surface y^+	1
Cells across tip gap (2% clr)	36
Inlet plane location (chords upstream of leading edge)	1.35
Exit plane location (chords downstream of trailing edge)	2.55

2 FIGURES

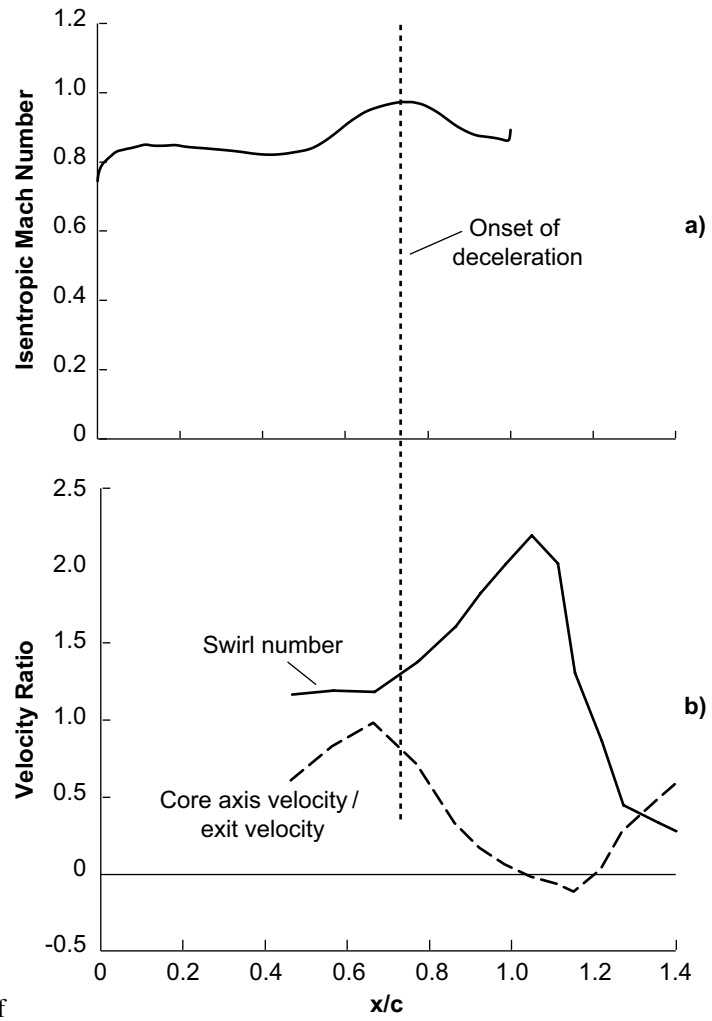
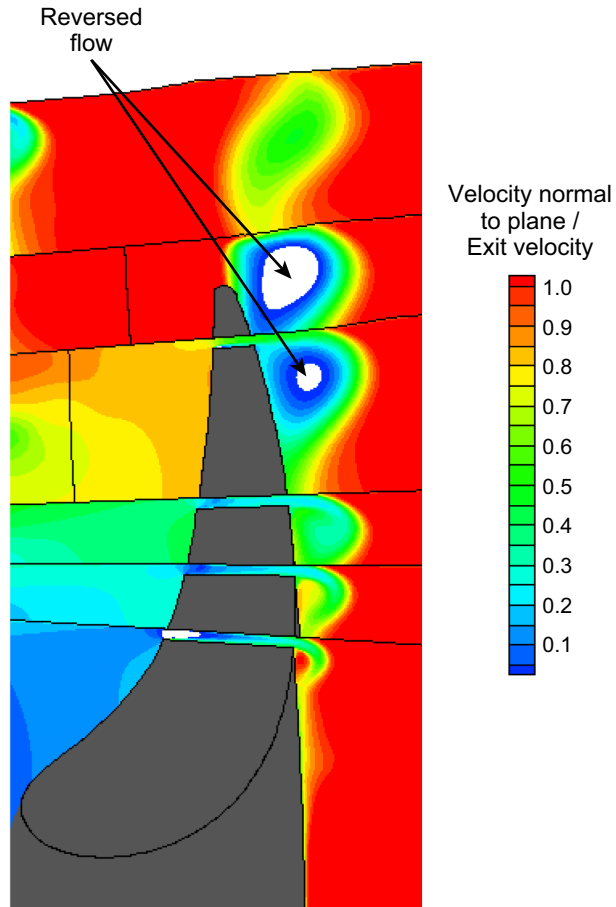
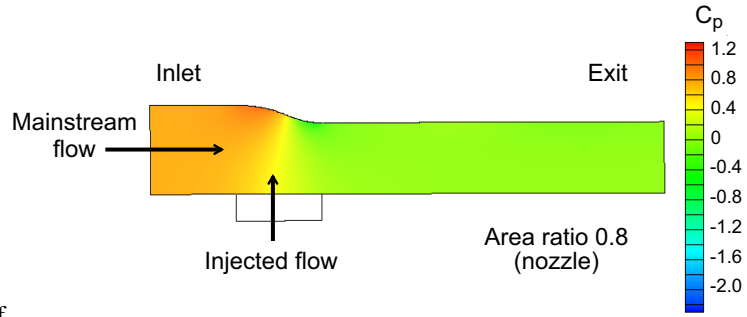


FIGURE 1. a) Suction surface isentropic Mach number at 80% span as a function of axial position. b) Vortex core swirl number ($\Gamma/2\pi r_c u_s$) and vortex centerline velocity normalize by exit velocity ($u_{s,centerline}/U_{exit}$) as a function of axial position



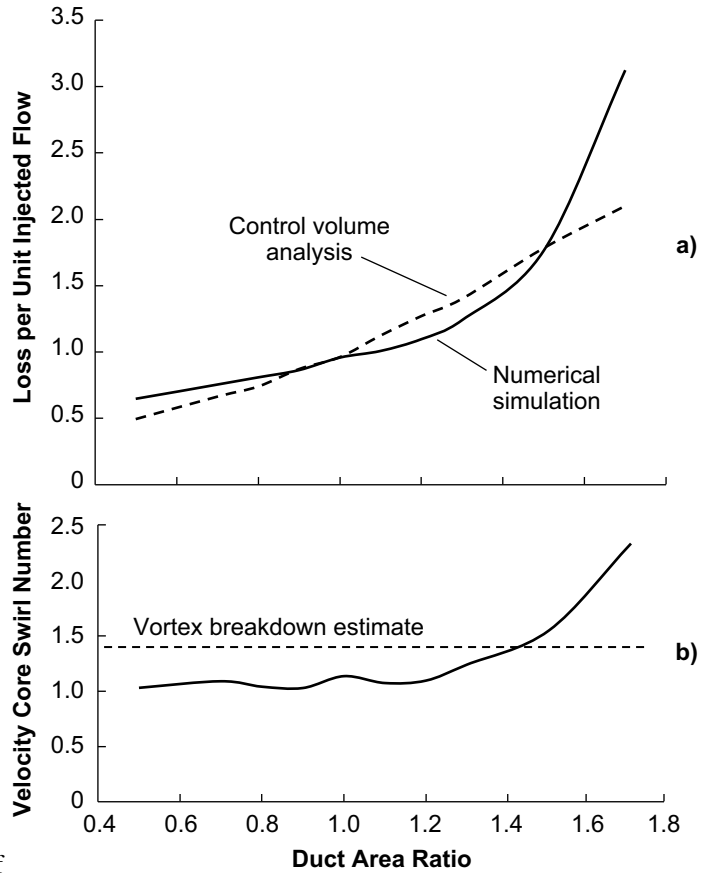
figs/fig2.pdf

FIGURE 2. Color contours of plane normal velocity / turbine exit velocity at different planes normal to the blade suction surface. The regions in which flow is reversed (negative core axis velocity) are indicated in white



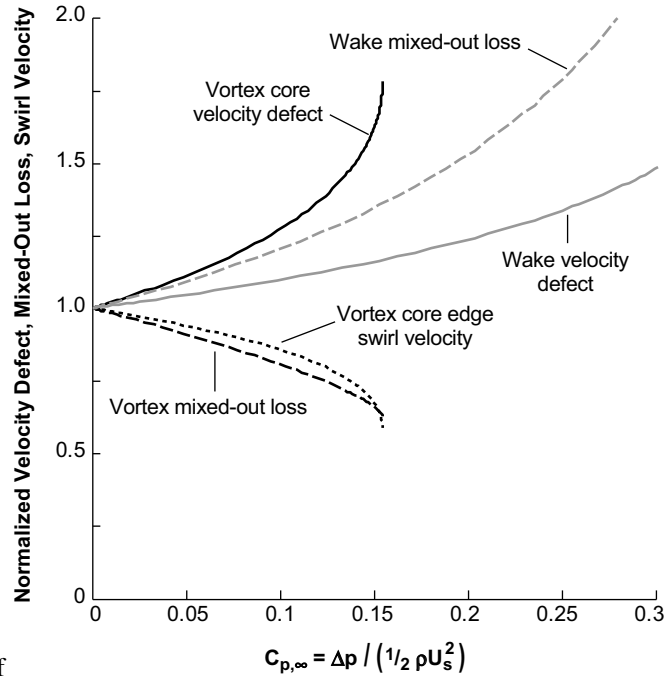
figs/fig3.pdf

FIGURE 3. Geometry of rectangular nozzle with area ratio 0.8. Color contours of static pressure coefficient $C_p = (p - p_{exit}) / \frac{1}{2} \rho u_{inlet}^2$



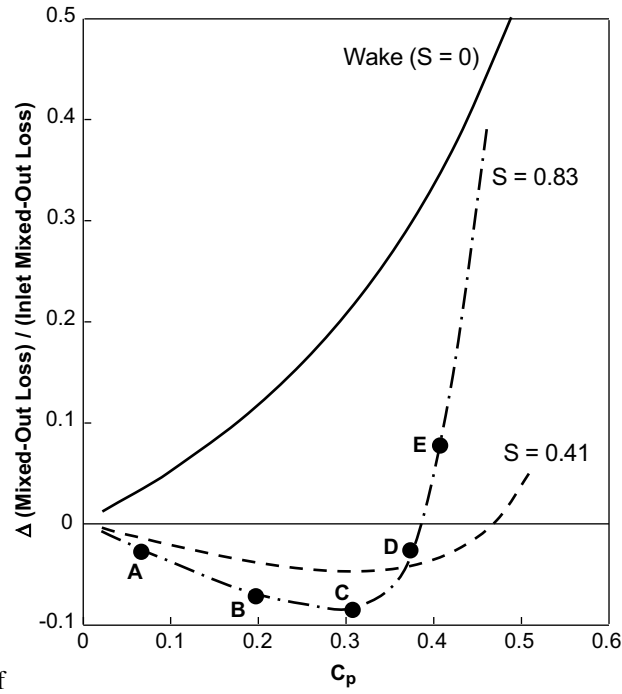
figs/fig4.pdf

FIGURE 4. **a)** Mixed out loss at duct exit, normalized by injected massflow and square of duct exit velocity, as a function of area ratio. Numerical simulation (solid line) and control volume approach (dotted line). **b)** Vortex swirl number at $x/H = 2$ for ducts with $AR = 0.5$ to 1.7 as a function of area ratio. Dotted line shows approximate vortex breakdown limit [14, 15]



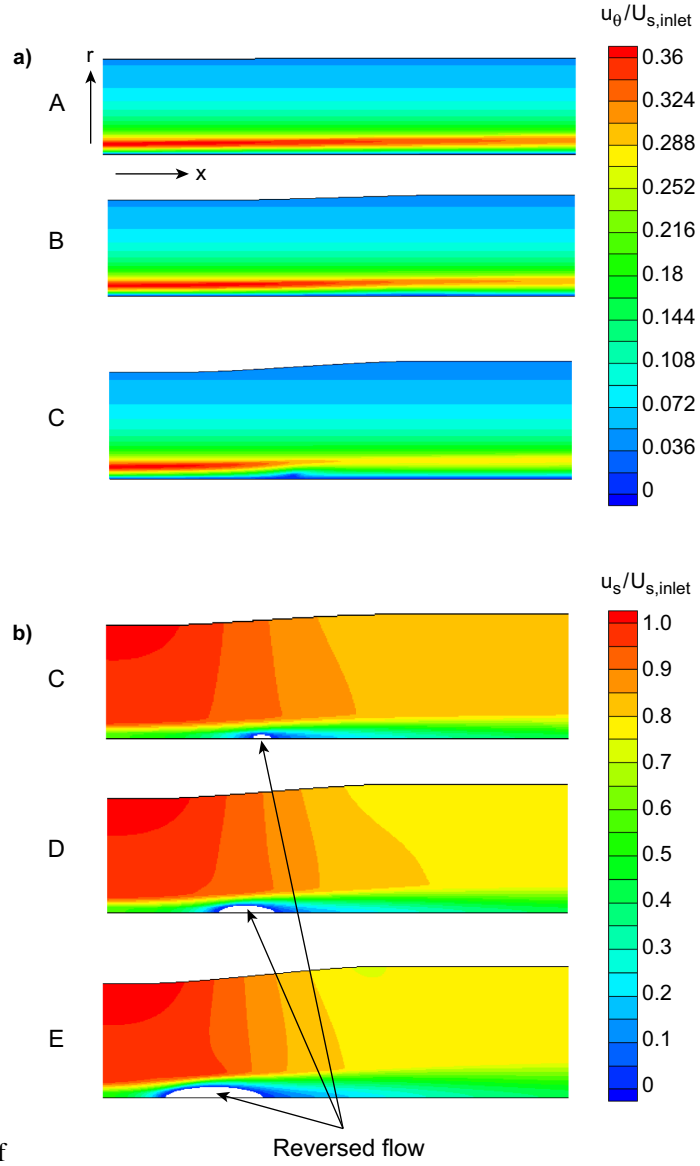
figs/fig5.pdf

FIGURE 5. Velocity defect, swirl velocity, and mixed-out loss (normalized by their inlet values) as a function of farfield pressure rise $C_{p,\infty}$ for inlet wake of velocity ratio 0.6 (black), and vortex of core axis velocity ratio $u_s/U_s = 0.6$ and swirl number $\Gamma/2\pi r_e u_s = 0.83$ (gray)



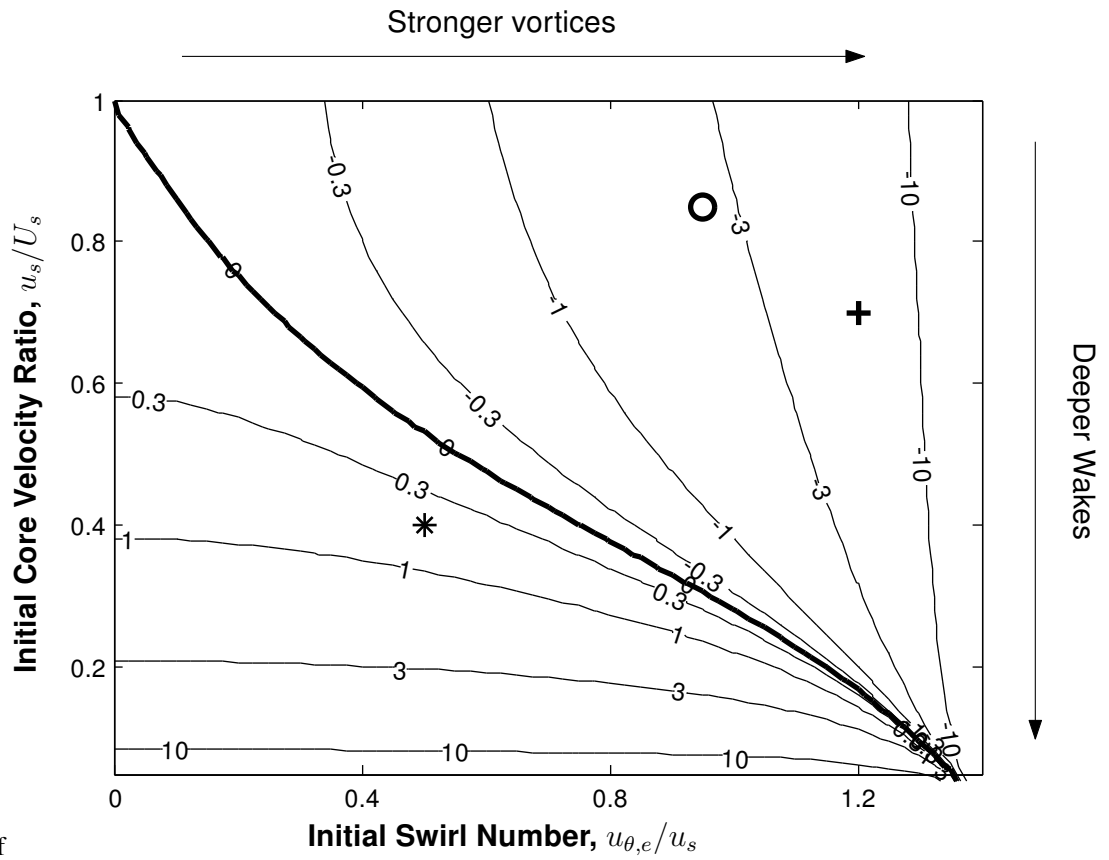
figs/fig6.pdf

FIGURE 6. Flow through expanding axisymmetric ducts. Mixed-out loss/inlet mixed-out loss for a wake and two vortices of differing swirl numbers (0.42 and 0.83) as a function of pressure rise on the outer wall $\Delta C_p = \Delta p / \frac{1}{2} \rho U_\infty^2$. The initial core velocity ratio in each case is. Velocity contours for cases A-E are shown in figure 7



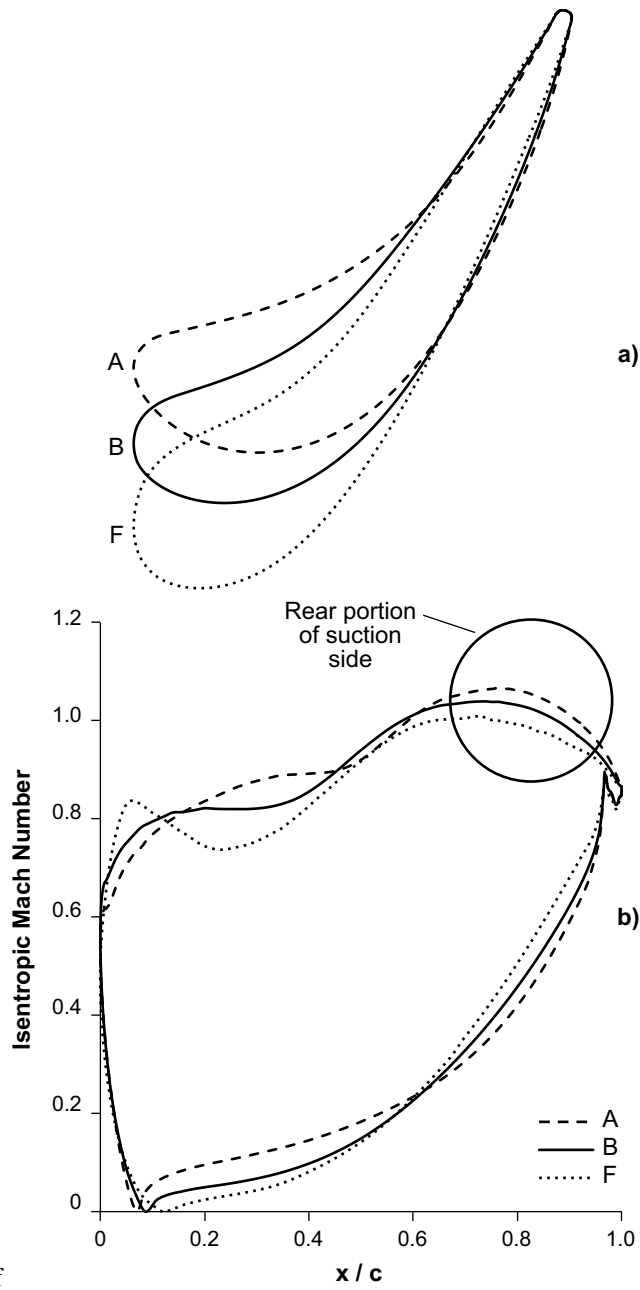
figs/fig7.pdf

FIGURE 7. **a)** Contours of $u_\theta / U_{s,inlet}$ for cases A, B and C (see figure 6; $\Delta C_p = 0.05, 0.19, 0.31$, $VR = 0.6$, $S = 0.83$). **b)** Contours of $u_s / U_{s,inlet}$ for cases C, D, and E ($\Delta C_p = 0.31, 0.37, 0.42$, $VR = 0.6$, $S = 0.83$). The regions in which flow is reversed (negative core axis velocity) are indicated in white



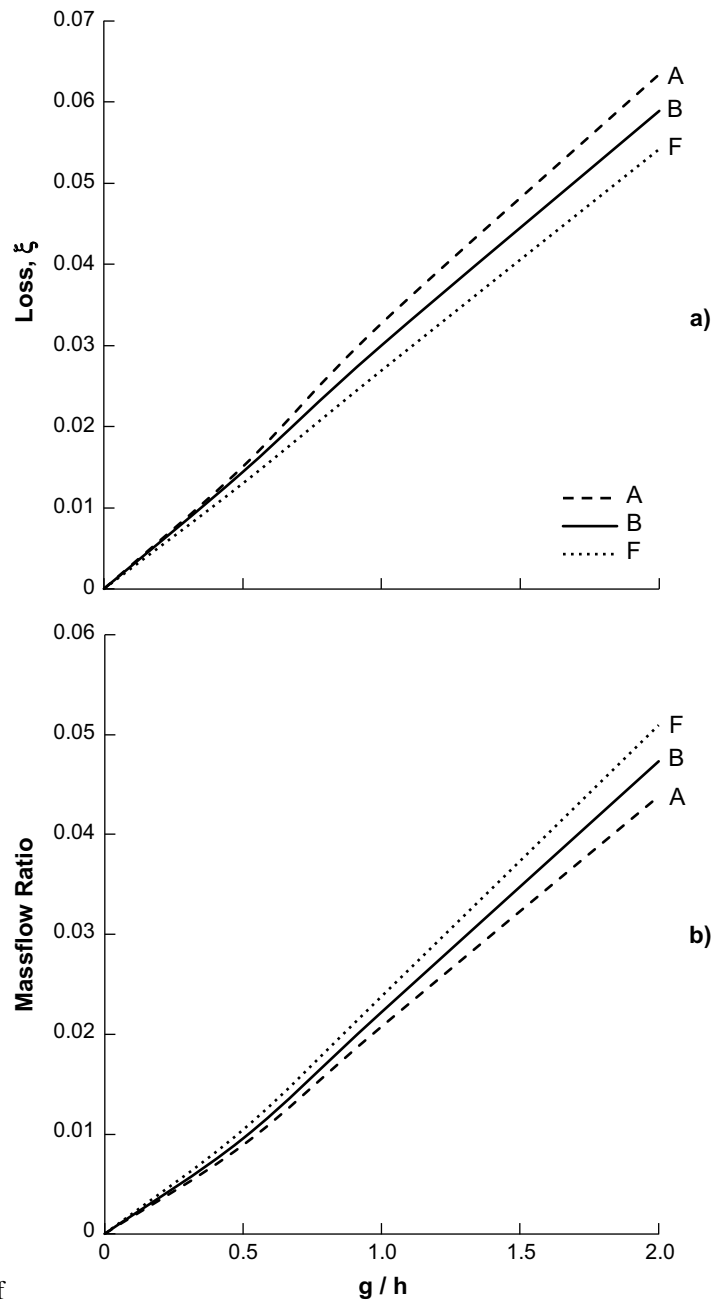
figs/fig8Oct22.pdf

FIGURE 8. Derivative of normalized mixed-out loss with respect to $C_{p,\infty}$, for vortices with specified initial swirl number and velocity ratio. Point represent low pressure turbine (\odot , computed), high pressure turbine ($+$, computed), and compressor experiments ($*$, [24])



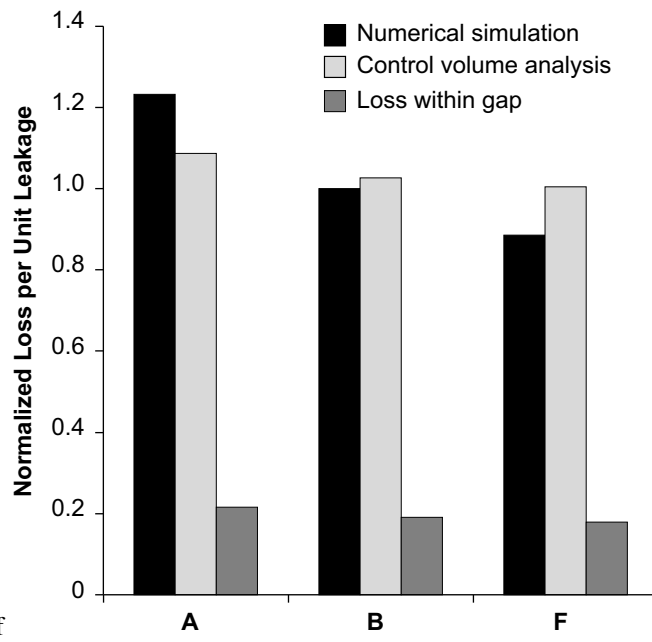
figs/fig9.pdf

FIGURE 9. a) Redesigned turbine tips (A,F) and baseline (B). b) Isentropic suction surface mach number at 80% span for A,B,F blades; clearance equal to 0.5% blade height



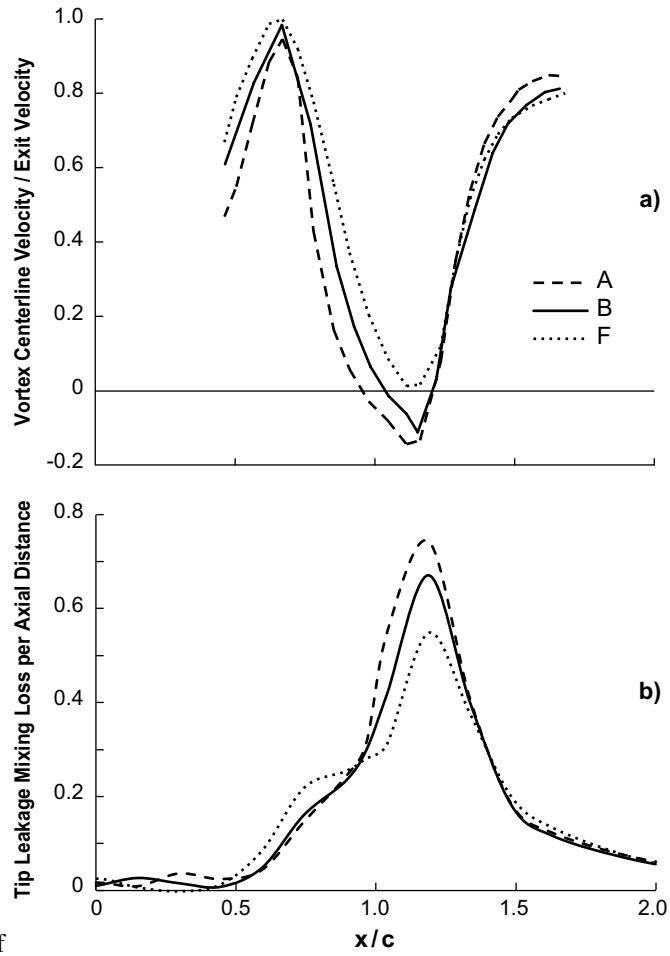
figs/fig10.pdf

FIGURE 10. a) Computed clearance loss coefficient ($T\Delta s_{leak}/\Delta h_t$) as a function of clearance for A, B, F BLADES. b) Leakage mass fraction ($\dot{m}_{leak}/\dot{m}_{main}$) as a function of clearance for A, B, F blades



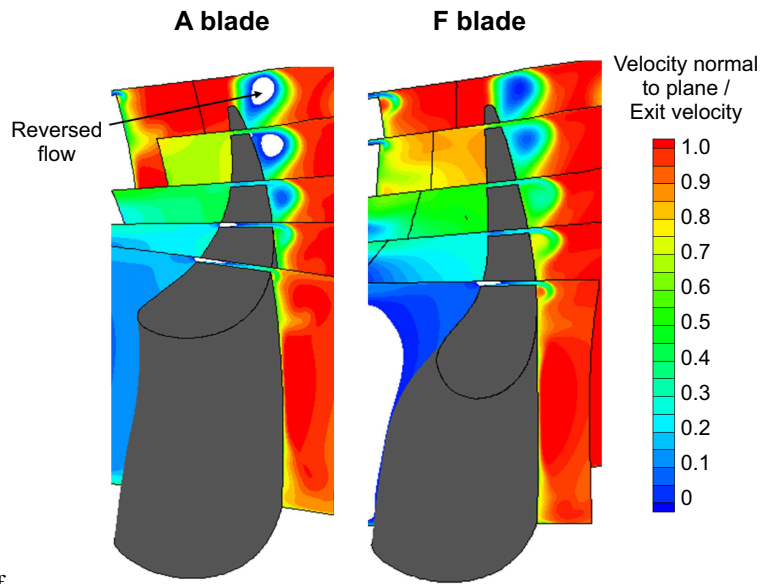
figs/fig11.pdf

FIGURE 11. Loss per unit leakage flow for A, B, F blades, from numerical simulations and from control volume estimate for mixing loss, normalized with respect to computed baseline loss per unit leakage flow; clearance equal to 2% blade height



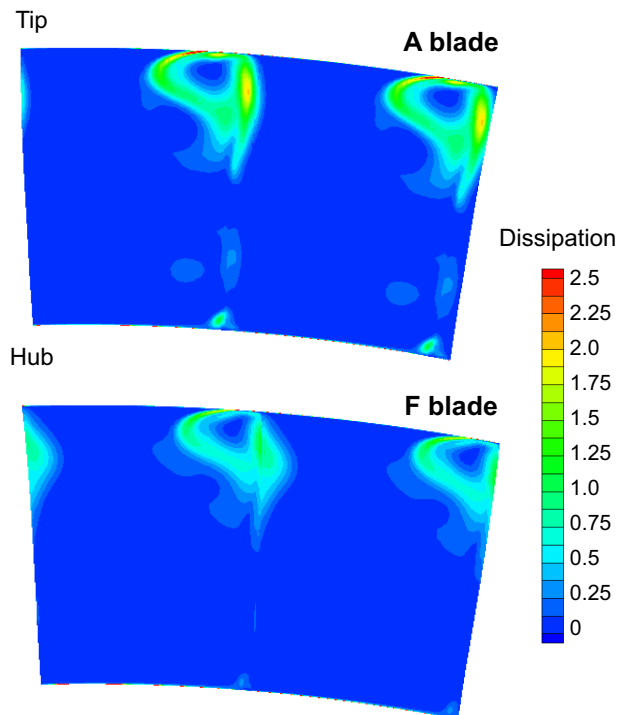
figs/fig12.pdf

FIGURE 12. a) Vortex centerline velocity normalized by exit velocity as a function of axial position for A, B, F blades; clearance equal to 2% of blade height. b) Tip leakage mixing loss per unit axial distance ($d\xi/d(x/c)$) as a function of axial position for A, B, F blades; clearance equal to 2% of blade height.



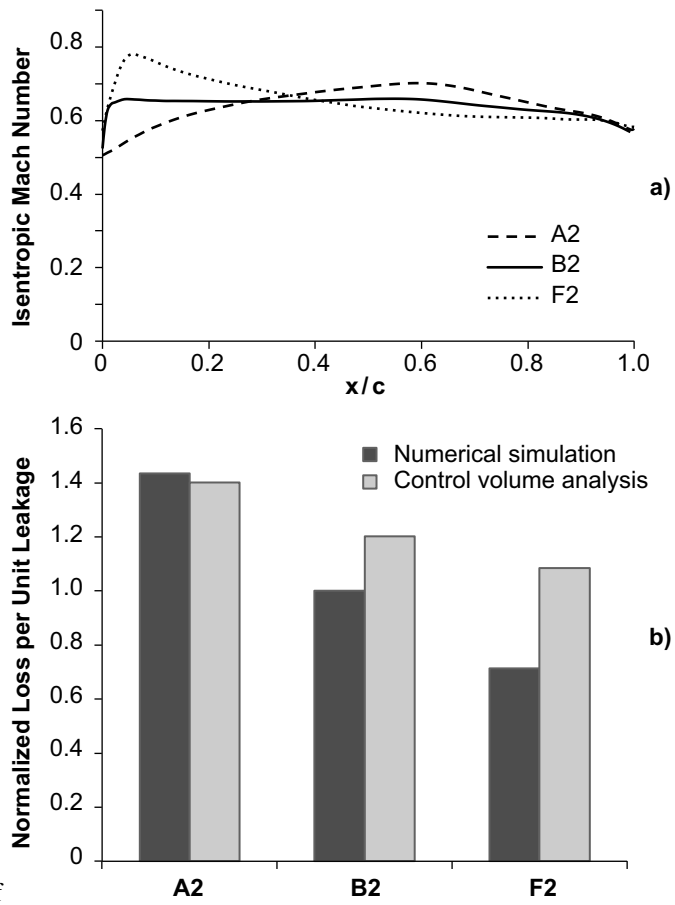
figs/fig13.pdf

FIGURE 13. Color contours of plane normal velocity/turbine exit velocity at several crossflow planes for A, F blades. Reversed flow regions are indicated in white



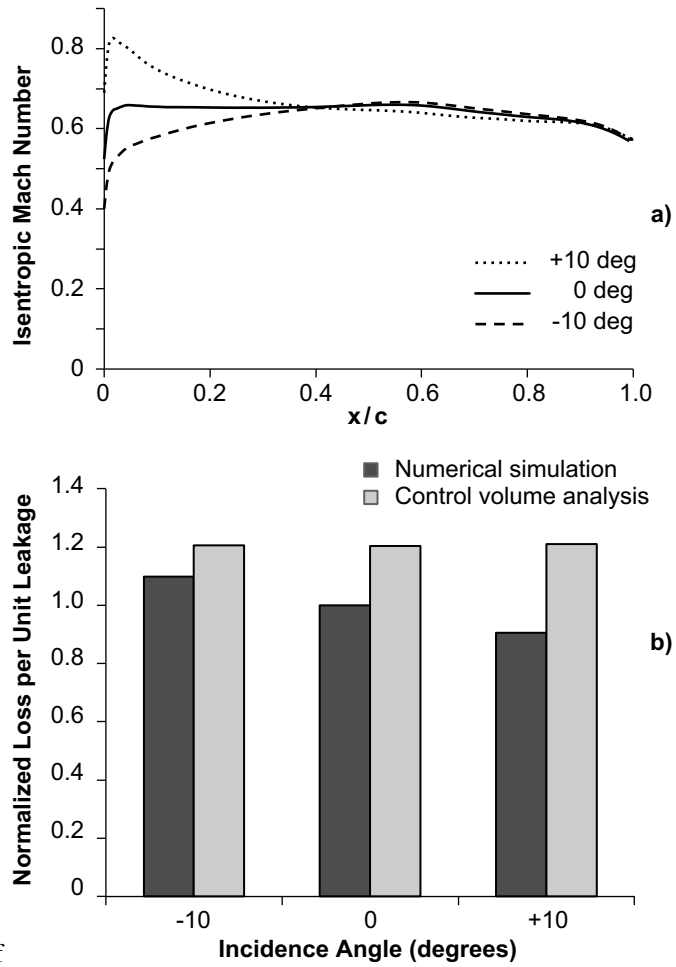
figs/fig14.pdf

FIGURE 14. fig14.eps



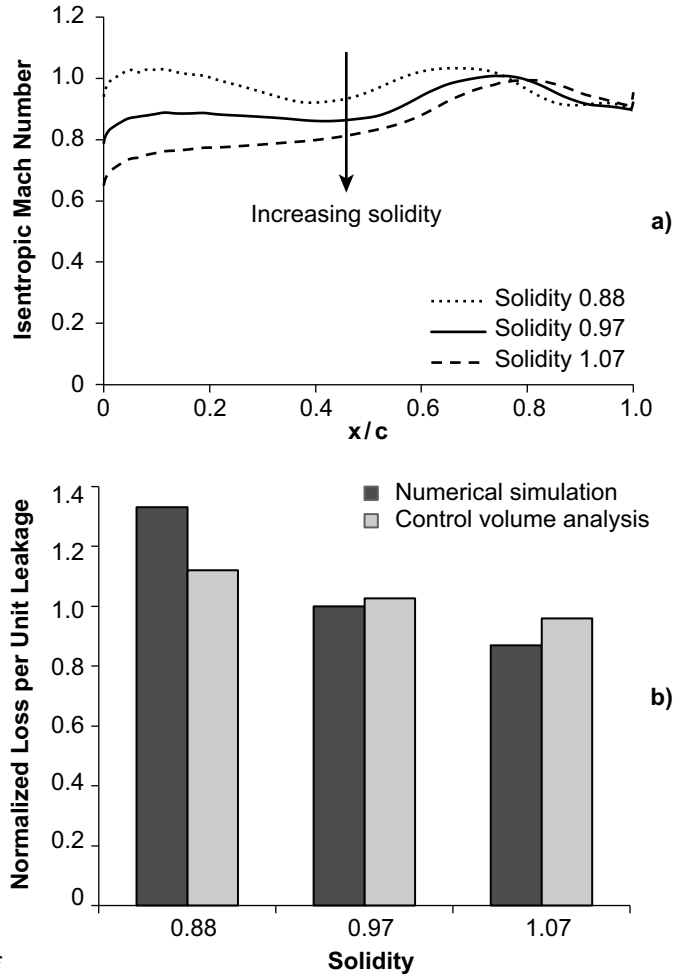
figs/fig15.pdf

FIGURE 15. a) Isentropic suction surface Mach number at 80% span for A2, B2, F2 blades. b) Loss per unit leakage flow for A2, B2, F2 blades, from numerical simulations and from control volume estimate for mixing loss, normalized with respect to computed baseline loss per unit leakage flow; clearance equal to 2% blade height



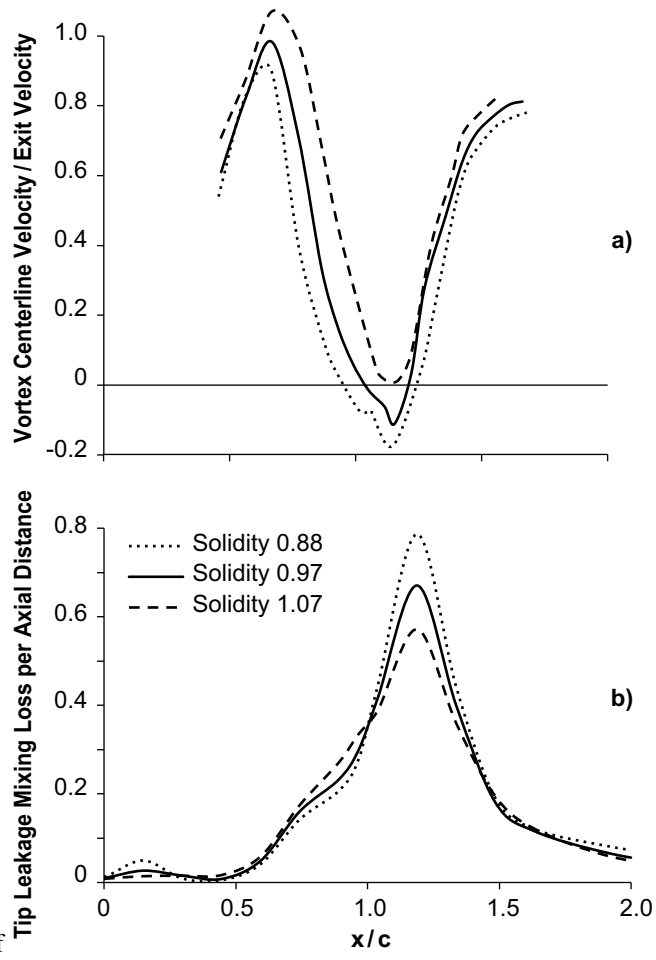
figs/fig16.pdf

FIGURE 16. a) Isentropic suction surface Mach number at 80% span for B2 at incidences of nominal, +10, and -10 degrees. b) Loss per unit leakage flow as a function of incidence for B2 blade, from numerical simulations and from control volume estimate for mixing loss, normalized with respect to computed baseline loss per unit leakage flow; clearance equal to 2% blade height



figs/fig17.pdf

FIGURE 17. a) Isentropic suction surface Mach number at 80% span for blades with solidity 0.88, 0.97, 1.07. b) Loss per unit leakage flow as a function of solidity, from numerical simulations and from control volume estimate for mixing loss, normalized with respect to computed baseline loss per unit leakage flow; clearance equal to 2% blade height



figs/fig18.pdf

FIGURE 18. a) Vortex core centerline velocity/cascade exit velocity as a function of axial position for blades with solidity 0.88, 0.97, AND 1.07. b) Normalized tip leakage loss per unit axial distance as a function of axial position